Study on the heat and mass transfer in ultrasonic assisting vacuum membrane distillation

Hao Guo[*1,2], Changsheng Peng[1], Weifang Ma[3], Hetao Yuan[1] and Ke Yang[1]

[1]*Key Laboratory of Marine Environment and Ecology, Ministry of Education, College of Environmental Science and Engineering, Ocean University of China, Qingdao 266100, P.R. China*
[2]*Beijing Institute of High-tech Environmental Science, Beijing 101111, P.R. China*
[3]*College of Environmental Science and Engineering, Beijing Forestry University, Beijing 100083, P.R. China*

Abstract. An ultrasonic assisting vacuum membrane distillation (VMD) system was designed to promote the heat and mass transfer in membrane distillation (MD) process. Both the effects of operating conditions and ultrasonic parameters to permeation flux in this process were investigated; the heat and mass transfer mechanism was also being discussed in this paper. The results showed that the performance of VMD process was improved significantly by ultrasonic assisting. The permeation flux was boosted at a certain feed solution temperature, pressure at permeate side and feed solution velocity whether or not to PP and PTFE. The results also indicated that ultrasonic power and frequency also was the key factor affecting the mass and transfer efficiencies. The feed side transfer coefficient (K_f), corresponding to ultrasonic power ($K_f=4.406-0.026\times P+7.824\times 10^{-5}\times P^2$) and ultrasonic frequency ($K_f=0.941+0.598\times f-0.012\times f^2+6.283\times 10^{-5} f^3$), was obtained and employed in the modeling of ultrasonic assisting VMD process. The modeling results showed that the calculated value of K_f aligned with experimental results well. Both variations of temperature polarization coefficient (*TPC*) and concentration polarization coefficient (*CPC*) were studied based on the obtained data. The results showed that both *TPC* and *CPC* were improved obviously by the ultrasonic parameters.

Keywords: vacuum membrane distillation; ultrasonic assisting; heat and mass transfer; permeation flux; transfer coefficient

1. Introduction

Membrane distillation (MD) is a separation process which combines with membrane and distillation technology, has employed in high salinity solutions desalination and nonvolatile components concentration (Chang *et al.* 2014, Lawson and Lloyd 1997, El-Bourawi *et al.* 2006, Alkhudhiri *et al.* 2012, Garcia-Payo *et al.* 2010). In MD process, water molecules or other volatile components were separated depending on the vapor pressure between two sides of porous hydrophobic membrane (Gryta 2010, Xu *et al.* 2006). Based on the distinction of vapor condensing in permeate side, different technologies have been developed, such as direct contact

---

∗Corresponding author, Ph.D., E-mail: guohao8432@126.com

membrane distillation (DCMD), sweeping gas membrane distillation (SGMD), air gap membrane distillation (AMD) and vacuum membrane distillation (VMD) (El-Bourawi *et al.* 2006, Loussif and Orfi 2016). VMD process has gained most attention and been developed rapidly since the permeate side remains vacuum state, the heat transfer via membrane can be ignored and possesses less heat loss. Yang et al. concluded the VMD performance depended upon the support materials which is used for PVDF membranes by the phase inversion technique (Yang *et al.* 2014, 2016). Chen et al. summarized the structure and VMD performance of PVDF composite membranes influenced upon the blending of PVDF materials (Chen *et al.* 2014, 2015). Efome et al. studied the enhanced VMD performance of superhydrophobic SiO₂ nano-particles blended PVDF flat sheet membranes prepared by the phase inversion technique for desalination applications (Efome *et al.* 2015, 2016). Diban et al. discussed the influence of feed solution temperature, pressure at permeate side and feed solution velocity to permeation flux (Diban *et al.* 2009, Banat *et al.* 2003). Schofield et al. achieved research of the heat and mass transfer of VMD process (Schofield *et al.* 1987, Lawson and Lloyd 1996). However, the permeation flux of VMD is lower than others MD process, hence physical assisted VMD to enhance mass transfer is an effective means (Cheng *et al.* 2008).

Ultrasonic assisting VMD to enhance mass transfer depends on turbulence of ultrasonic cavitation effects. The cavitation bubbles were expanded and collapsed under the ultrasonic and evoked liquid phase turbulence, the thickness of liquid boundary which caused the concentration and temperature polarization changed thin and promoted the mass transfer (Liu *et al.* 2008). At present, the application effects and influence factors of ultrasonic assisting VMD were researched widely (Chiam and Sarbatly 2013, Abu-Zeid *et al.* 2016, Cao *et al.* 2016); however the mechanism of ultrasonic promoting heat and mass transfer was studied neglected. In this article, solution temperatures, superficial velocity, permeate side vacuum, ultrasonic power and frequency influence on permeation flux have been researched primarily. The mathematical model of ultrasonic parameters against mass transfer has been established. Both variations of concentration polarization coefficient CPC and temperature polarization coefficient TPC toward ultrasonic parameters also analyzed.

2. Theory

The heat and mass transfer principally was divided into three steps, (1) transfer from the feed bulk to the membrane surface (feed side); (2) transfer through the membrane pores from the feed to permeate side; (3) transfer from the membrane surface (permeate side) to permeate bulk (Loussif and Orfi 2014, Mengual *et al.* 2004).

2.1 Heat transfer

In VMD process, the heat transfer from feed bulk to membrane surface (feed side); Q_f(W) is calculated as Eq. (1).

$$Q_f = h_f A_f (T_f - T_{fm}) \tag{1}$$

where h_f (W·m⁻²·K⁻¹) is the heat transfer coefficient of feed bulk; A_f (m²) is the effective inner surface area of the hollow fiber membrane and calculated from Eq. (2); T_f(K) is temperature of

feed bulk; $T_{fm}(K)$ is temperature of membrane surface (feed side).

$$A_f = \pi d l \tag{2}$$

where $d(m)$ is the inner diameter of hollow fiber membrane; $l(m)$ is the length of hollow fiber membrane.

The over heat-transfer flux across the membrane, $Q_m(W)$ is expressed via Eq. (3). The contribution of the heat conduct through the membrane matrix can be neglected due to the high vacuum degree in the permeate side; therefore Eq. (3) can be simplified to Eq. (4).

$$Q_m = J\Delta H A_m + \frac{h_f}{\delta} A_m \left(T_{fm} - T_{pm}\right) \tag{3}$$

$$Q_m = J\Delta H A_m \tag{4}$$

where J (kg·m^{-2}·h^{-1}) is the flux of VMD; ΔH (J·kg^{-1}) is the latent heat of vapor at temperature of $T_{fm}(K)$ and it can be calculated as Eq. (5); A_m (m^2) is the effective area of the transmembrane heat transfer and it can be expressed as Eq. (6); $T_{pm}(K)$ is temperature of membrane surface (permeate side) (Li and Sirkar 2005).

$$\Delta H = 2258.4 + 2.47\left(373 - T_{fm}\right) \tag{5}$$

$$A_m = \pi \frac{D - d}{\ln\frac{D}{d}} L \tag{6}$$

where $D(m)$ stands for the external diameter of hollow fiber membrane.

For the condition of phase flow is laminar in hollow fiber membrane, h_f (W·m^{-2}·K^{-1}) can be calculated from Eq. (7) with the correlations between Nusselt (Nu), Reynolds (Re) and Prandtl (Pr) dimensionless numbers.

$$Nu = 1.86 Re^{1/3} Pr^{1/3} \left(\frac{d}{L}\right)^{1/3} \left(\frac{\mu_f}{\mu_w}\right)^{0.14}$$

$$Nu = \frac{h_f d}{\lambda}, Re = \frac{u\rho d}{\mu_f}, Pr = \frac{c_p \mu_f}{\lambda} \tag{7}$$

where μ_f (kg·m^{-1}·s^{-1}) and μ_w (kg·m^{-1}·s^{-1}) represents for the dynamic viscosity of feed bulk and water; λ (W·m^{-1}·K^{-1}) is the thermal conductivity of feed bulk; u (m·s^{-1}) is the superficial velocity of feed bulk; ρ (kg·m^{-3}) is the density of the feed solution; c_p (J·kg^{-1}·K^{-1}) is the heat capacity at constant pressure of the feed solution (Chiam and Sarbatly 2013, Abu-Zeid *et al.* 2016).

The $T_{fm}(K)$ value can be deduced from $Q_f = Q_m$ and calculated as Eq. (8).

$$T_{fm} = T_f - \frac{J\Delta H A_m}{h_f A_f} \tag{8}$$

Furthermore, the temperature polarization coefficient (TPC) is defined as Eq. (9).

$$TPC = \frac{T_{fm}}{T_f} \tag{9}$$

The TPC value is used to measure the effect of heat transfer through a boundary layer to the total heat transfer resistance of the system. When the thermal boundary layer resistance is reduced, the temperature difference between the feed bulk and the membrane surface is almost equivalent (Banat *et al.* 2015, Al-Asheh *et al.* 2006, Mericq *et al.* 2011).

2.2 Mass transfer

The permeation flux J (kg·m^{-2}·h^{-1}) of VMD can be calculated as Eq. (10). Δp (Pa) is the differential pressure between membrane surface (feed side) and membrane surface (permeate side), Δp (Pa) can be calculated from Eq. (11).

$$J = K_T \cdot \Delta p \tag{10}$$

$$\Delta p = p_{fm} - p_p \tag{11}$$

where K_T (kg·m^{-2}·s^{-1}·Pa^{-1}) represents for the total mass transfer; p_{fm} is the water vapor pressure at membrane surface (feed side) and be expressed as Eq. (12); p_p is the pressure at permeate side (Fick 1995).

$$p_{fm} = \exp\left(23.238 - \frac{3841}{T_{fm} - 45}\right)\left(1 - x_{fm}\right)\left(1 - 0.5x_{fm} - 10x_{fm}^2\right) \tag{12}$$

where value x_{fm} is the salt molar fraction of feed solution (Schofield *et al.* 1987).

For the mass transfer is divided into three steps, K_T can be defined as Eq. (13).

$$\frac{1}{K_T} = \frac{1}{K_f} + \frac{1}{K_m} + \frac{1}{K_p} \tag{13}$$

where K_f, K_m and K_p represents for feed side, transmembrane and permeate side mass transfer coefficient respectively.

The contribution of K_p can be neglected due to the high vacuum degree in the permeate side ($K_p \gg K_f, K_m$); therefore Eq. (13) can be simplified to Eq. (14) (Wang *et al.* 2014).

$$\frac{1}{K_T} = \frac{1}{K_f} + \frac{1}{K_m} \tag{14}$$

For VMD process, both Knudsen diffusion ($K_{knudsen}$) and Poiseuille flow ($K_{viscous}$) make contributions to transmembrane mass transfer (K_m). Value K_m (kg·m^{-2}·s^{-1}·Pa^{-1}) can be expressed as Eq. (13).

$$K_m = 1.064 \frac{r\varepsilon}{\tau\delta} \sqrt{\frac{M}{RT_m}} + 0.125 \frac{r^2\varepsilon}{\tau\delta} \frac{Mp_m}{\mu RT_m} \tag{15}$$

where $r(m)$, $\varepsilon(-)$, $\tau(-)$ and $\delta(m)$ respectively represents for pore radius, porosity, pore tortuosity factor and thickness of membrane. M (18.02 kg·kmol^{-1}) is the molecular weight of water, μ (Pa·s^{-1}) is viscosity of water vapor, R (8.314×10^3 J·kmol^{-1}·K^{-1}) is the universal gas constant. $T_m(K)$, p_m (Pa) is the average temperature and average vapor pressure in membrane pores and defined as Eq. (16) and Eq. (17).

$$T_m = \frac{(T_{fm} + T_p)}{2} \tag{16}$$

$$p_m = \frac{(p_{fm} + p_p)}{2} \tag{17}$$

Furthermore, the concentration polarization coefficient (CPC) is defined as Eq. (18). CPC is defined to quantify the mass transport resistance within the concentration boundary layer on the feed side, when the concentration boundary layer is reduced, the concentration difference between the feed bulk and the membrane surface is also decreased, consequently the mass transport process is improved.

$$CPC = \frac{c_{fm}}{c_f} = \exp\left(\frac{J}{\rho K_f}\right) \tag{18}$$

where c_{fm} (mol·L^{-1}) and c_f (mol·L^{-1}) is the molar concentration of feed solution on membrane surface (feed side) and feed bulk (Porter 1972).

3. Experimental

3.1 Materials and equipment

Ultrasonic assisting VMD equipment was fabricated by our research group. The temperature of feed bulk was maintained by thermostatic water bath (HH.S21-6, Shanghai Boxun Co. Ltd. China). The salinity of feed solution was 3.5% (wt.) and prepared by sea salts (Beijing Salt Industry Corporation, CNSG). Mercurial thermometers with an accuracy of ±0.1℃ were used for measuring the inlet and outlet temperature of feed flow. Electronic balance with accuracy of ±0.1g was used for measuring the weight of product water.

Two types porous hydrophobic hollow fiber membrane were employed in this study. Propene polymer (PP) and Polytetrafluoroethylene (PTFE) membranes were provided by Membrana GmbH and Dongda Water Group Co. Ltd. respectively. The relevant membrane parameters and membrane module specifications were listed in Table 1 and Table 2 respectively.

PP (phase inversion membrane)

$$\tau = \frac{(2 - \varepsilon)^2}{\varepsilon} \tag{19}$$

PTFE (stretching membrane)

Table 1 Parameters of PP and PTFE hollow fiber membrane

Membrane material	Inner diameter d (mm)	Outer diameter D (mm)	Thickness δ (mm)	Pore radius r (μm)	Porosity ε(-)	Tortuosity factor τ(-)*
PP	1.66	2.41	0.375	0.231	80	1.8
PTFE	0.8	1.7	0.45	0.1	65	1.54

*Tortuosity factor was calculated from Eq. (19) and Eq. (20).

Table 2 Specifications of PP and PTFE membrane module

Membrane module	Amount of membrane fiber n(-)	Effective length of membrane module l (mm)	Effective area of membrane inner side A_f (m^2)	Effective area of heat transfer via membrane A_m (m^2)
PP	16	200	0.017	0.02
PTFE	40	200	0.02	0.03
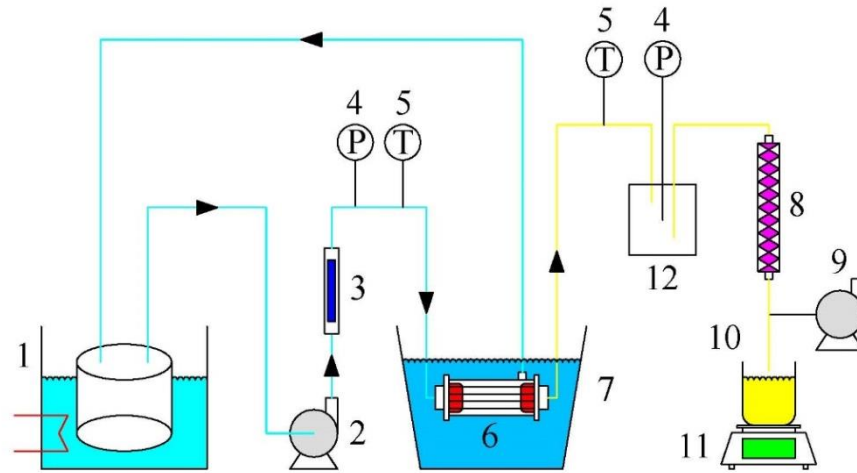
Fig. 1 Flow chart of ultrasonic assisting VMD equipment. 1. Thermostatic water bath; 2. Magnetic drive pump; 3. Liquid flowmeter; 4. Manometer; 5. Thermometer; 6. Hollow fiber membrane module; 7. Ultrasonic cleaning tank; 8. Condenser; 9. Vacuum pump; 10. Product collection tank; 11. Electronic balance; 12. Buffer bottle

$$\tau = \frac{1}{\varepsilon} \tag{20}$$

3.2 Experimental setup and operation method

The flow chart of ultrasonic assisting VMD equipment was shown in Fig. 1. Feed solution temperature was maintained constant from the thermostatic water bath and circulated through the membrane module by a magnetic drive pump. The velocity of feed solution was controlled and monitored by liquid flowmeter. A vacuum pump with a pressure controller was connected to the shell side of the membrane module to remove the permeation vapor. The water vapor pressure in the vacuum side was measured by a vacuum gauge. Each experiment was repeated three times and all data were the average of the repeats.

The weight of product water W (kg) was measured by electronic balance and the permeation flux J (kg·m^{-2}·h^{-1}) was calculated as Eq. (21).

$$J = \frac{W}{A_f t} \tag{21}$$

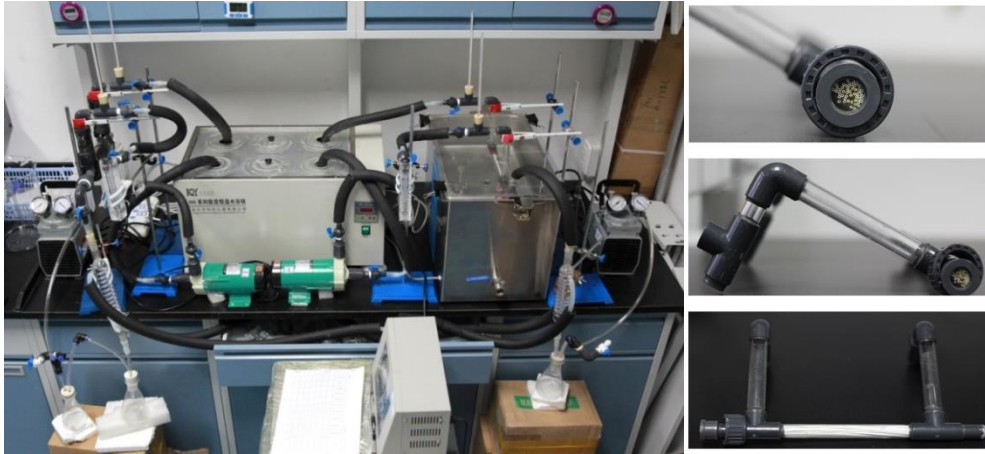where t(h) represents for the working time of equipment.

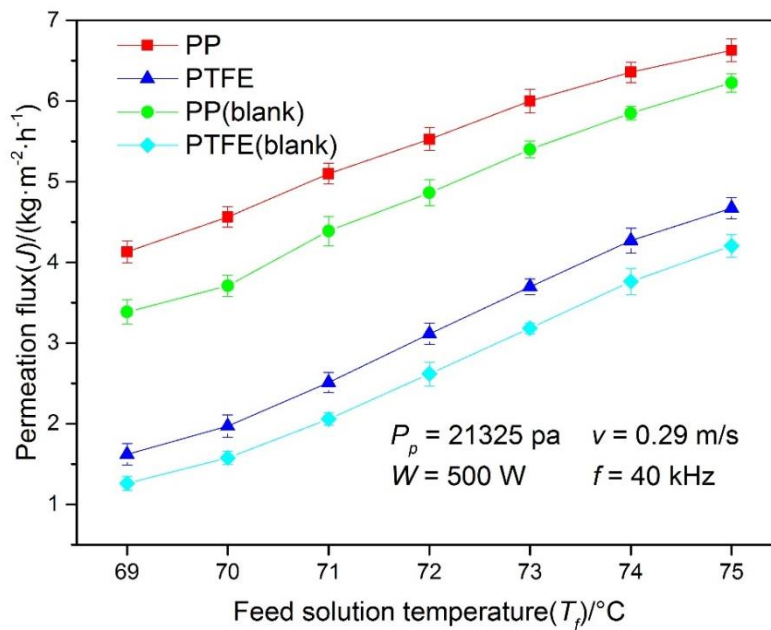Fig. 2 Photograph of ultrasonic assisting VMD equipment and membrane module

Fig. 3 Effect of the feed solution temperature to permeation flux

4. Results and discussion

4.1 Effect of operating conditions to permeation flux

4.1.1 Feed solution temperature

Fig. 3 showed that the permeation flux of PP and PTFE hollow fiber membrane changed with different feed solution temperature when operating under certain conditions. According to this experiment, permeation flux increased with feed solution temperature. This phenomenon due to the water vapor pressure relates with the permeation flux, on the base of Antoine equation, water
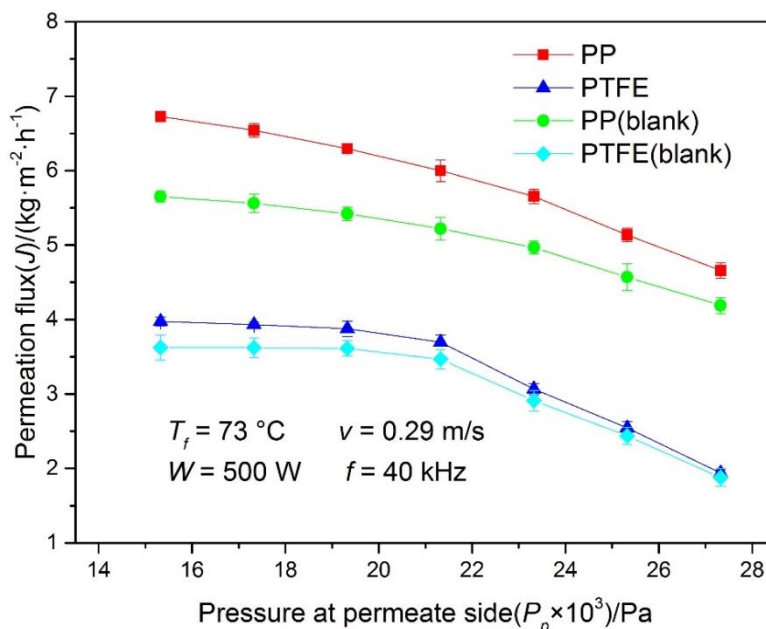
Fig. 4 Effect of the pressure at permeate side to permeation flux

vapor pressure increase with the with the solution temperature. For VMD process, the driving force of permeation is simultaneously determined by the water vapor pressure at feed side and pressure at permeate side. In accordance with Eqs. (10) and (11), the permeation flux increase with the discrepancy between p_{fm} and p_p value.

4.1.2 Pressure at permeate side

Fig. 4 showed that the permeation flux of PP and PTFE hollow fiber membrane changed with different pressure at permeate side when operating under certain conditions. Similar to Fig. 3, the permeation flux of PP membrane was superior to PTFE membrane. Because of the same reason as 4.1.1, when the feed solution temperature maintained constant, the driving force of permeation changed only related with the pressure at permeate side. In addition, the permeation flux decreased with the pressure at permeates side according to Eqs. (10) and (11). However, the lower pressure at permeate side might cause the moistening phenomenon of hydrophobic membrane and resulted in salt rejection decreased.

4.1.3 Feed solution velocity

Fig. 5 showed that the permeation flux of PP and PTFE hollow fiber membrane changed with different feed solution velocity when operating under certain conditions. It is different from feed solution temperature and pressure at permeate side directly influenced the driving force of permeation, the feed solution velocity improved the feed flow state so that the transmembrane mass transfer was accelerated. Furthermore, the permeation flux increased with the feed solution velocity on account of the higher turbulence degree reduced the thickness of thermal boundary layer. For this reason, the temperature of membrane surface (feed side) was enhanced indirectly; the permeation flux was also advanced in accordance with 4.1.1.
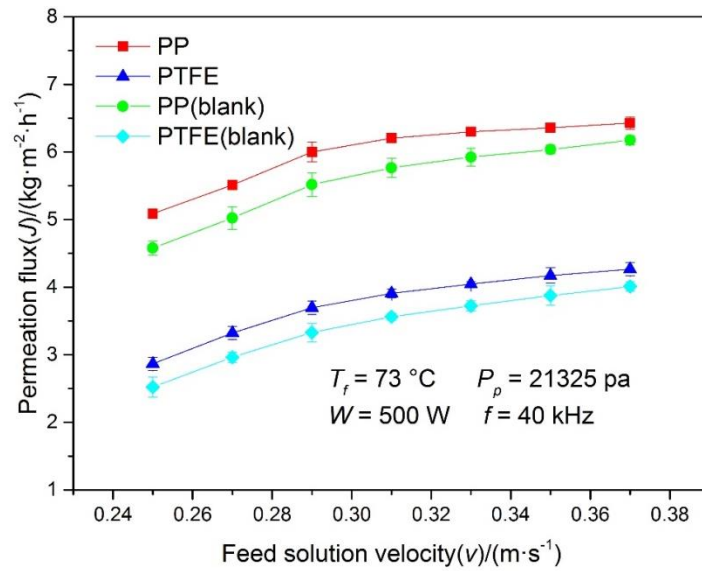
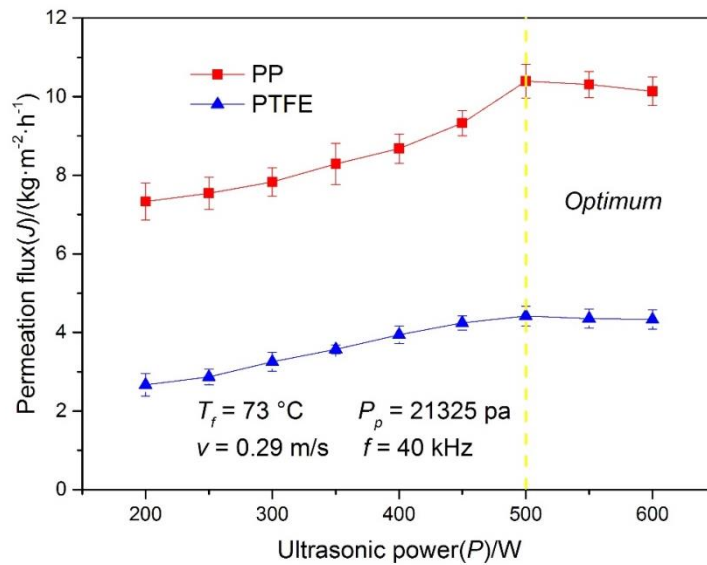Fig. 5 Effect of the feed solution velocity to permeation flux

Fig. 6 Effect of the ultrasonic power to permeation flux

4.2 Effect of ultrasonic parameters to permeation flux

4.2.1 Ultrasonic power

Fig. 6 showed that the permeation flux of PP and PTFE hollow fiber membrane changed with ultrasonic power when operating under certain conditions. The results shows that the permeation flux which is 10.39 kg·m^{-2}·h^{-1} (PP) and 4.42 kg·m^{-2}·h^{-1} (PTFE) reaches a maximum when the ultrasonic power is 500W. In addition, the tendency of this curve has been divided into two stages.
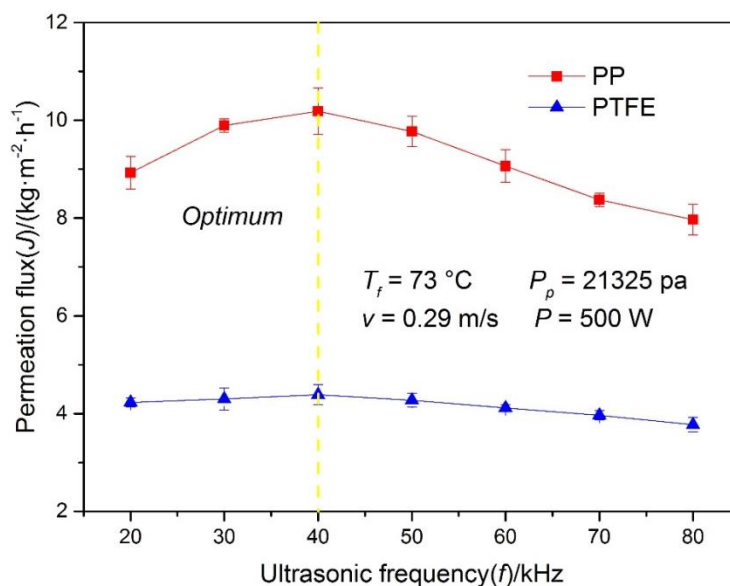
Fig. 7 Effect of the ultrasonic frequency to permeation flux

When the ultrasonic power is less than 500W, the permeation flux has been enhanced with the ultrasonic power increasing. Otherwise, the permeation flux was reduced gradually with the ultrasonic power increasing. It is indicates that higer ultrasonic power will promote the advance of permeation flux due to the ultrasonic cavitation effects has been strengthened, whereas extravagant ultrasonic power will lead to the cavitation bubbles connecting so as to the transmisson of sound wave was resist (Thompson and Doraiswamy 1999).

4.2.2 Ultrasonic frequency

Fig. 7 showed that the permeation flux of PP and PTFE hollow fiber membrane changed with ultrasonic frequency when operating under certain conditions. Similar to Fig. 6, the permeation flux of PP membrane was superior to PTFE membrane. The results shows that the permeation flux which is 10.19 kg$\cdot$m$^{-2}\cdot$h^{-1} (PP) and 4.39 kg$\cdot$m$^{-2}\cdot$h^{-1} (PTFE) reaches a maximum when the ultrasonic frequency is 40 kHz. In addition, the tendency of this curve also has been divided into two stages. When the ultrasonic frequency is less than 40kHz, the permeation flux has been enhanced with the ultrasonic frequency increasing. Otherwise, the permeation flux was reduced gradually with the ultrasonic frequency increasing. It is indicates that lower ultrasonic frequency will obtained preferable permeation flux due to the ultrasonic cavitation effects has been induced readily, whereas a large number of small volume cavitation bubbles generate at higher ultrasonic frequency and collapse along with lower energy (Crum 1995).

4.3 Feed side transfer coefficient

4.3.1 Calculation

In order to deduce K_f-P and K_f-f theoretical curves, the implicit equations containing only K_f and P, K_f and f were needed. Based on J-P and J-f curves from experimental data as

above research, meanwhile making use of Eq. (10) and Eq. (14), the theoretical curves which K_f-P and K_f-f were drawn as below. Fig. 8 showed the calculation flow chart of these implicit equations.

4.3.2 Effect of ultrasonic power to K_f

Fig. 9 showed that the feed side transfer coefficient of PP and PTFE hollow fiber membrane changed with ultrasonic power when operating under certain conditions (T_f=73°C; p_p=21325 Pa; v=0.29 m·s^{-1}; f=40 kHz). It is obviously shown that the curves of ultrasonic power to feed side transfer coefficient was divided into two parts. When the ultrasonic power was less than 500W, the
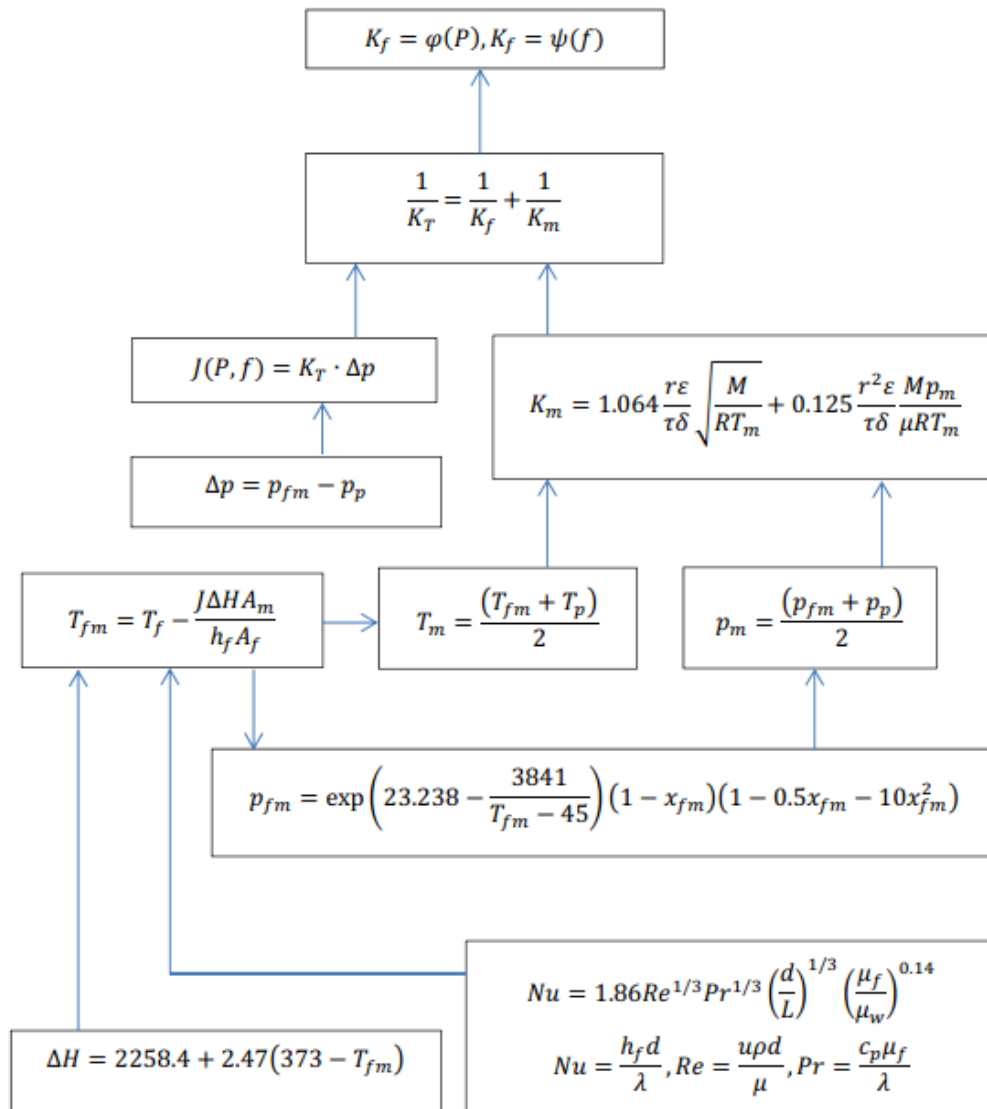
$$K_f = \varphi(P), K_f = \psi(f)$$

$$\frac{1}{K_T} = \frac{1}{K_f} + \frac{1}{K_m}$$

$$J(P,f) = K_T \cdot \Delta p$$

$$K_m = 1.064 \frac{r\varepsilon}{\tau\delta}\sqrt{\frac{M}{RT_m}} + 0.125 \frac{r^2\varepsilon}{\tau\delta}\frac{Mp_m}{\mu RT_m}$$

$$\Delta p = p_{fm} - p_p$$

$$T_{fm} = T_f - \frac{J\Delta H A_m}{h_f A_f}$$

$$T_m = \frac{(T_{fm} + T_p)}{2}$$

$$p_m = \frac{(p_{fm} + p_p)}{2}$$

$$p_{fm} = \exp\left(23.238 - \frac{3841}{T_{fm} - 45}\right)(1 - x_{fm})(1 - 0.5x_{fm} - 10x_{fm}^2)$$

$$\Delta H = 2258.4 + 2.47(373 - T_{fm})$$

$$Nu = 1.86Re^{1/3}Pr^{1/3}\left(\frac{d}{L}\right)^{1/3}\left(\frac{\mu_f}{\mu_w}\right)^{0.14}$$

$$Nu = \frac{h_f d}{\lambda}, Re = \frac{u\rho d}{\mu}, Pr = \frac{c_p\mu_f}{\lambda}$$

Fig. 8 Calculation flow chart of equations implicit containing only K_f and P, K_f and f
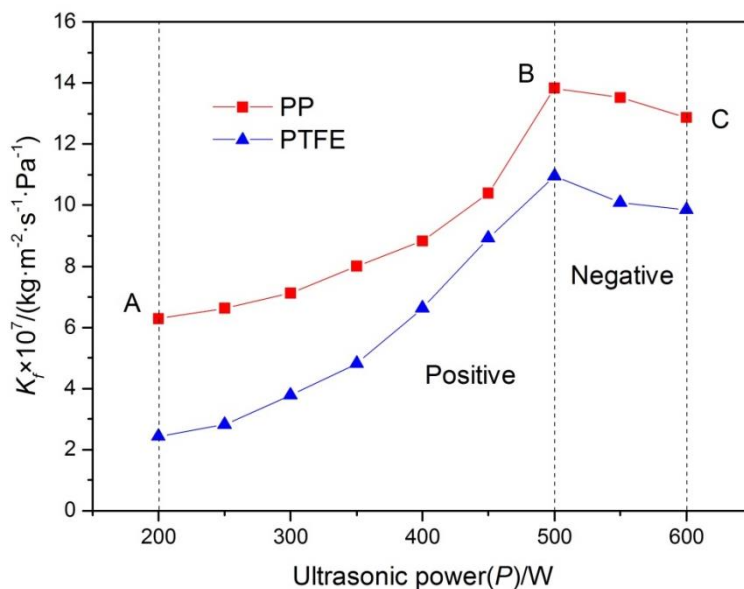
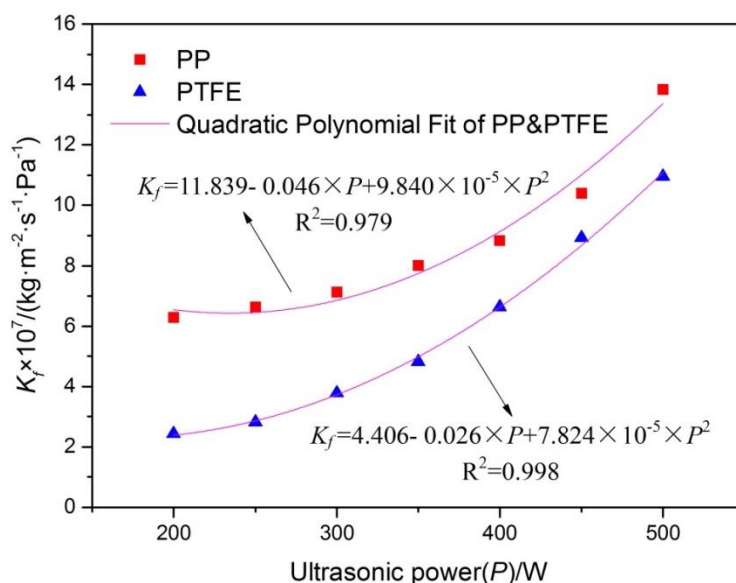Fig. 9 Effect of ultrasonic power to feed side transfer coefficient

Fig. 10 Relationship between feed side transfer coefficient and ultrasonic power

effect was positive; when the ultrasonic power was greater than 500W, the effect was negative. This phenomenon was because that the extravagant ultrasonic power was leading to the cavitation bubbles connecting so as to the transmission of sound wave was resist, the intensity of sound wave on membrane surface (feed side) was greatly reduced and the turbulence degree was get worse, hence the transfer coefficient was unsatisfactory.

Fig. 10 showed the quadratic polynomial fit for feed side transfer coefficient of PP and PTFE

hollow fiber membrane changed with ultrasonic power (P<500W) when operating under certain conditions (T_f=73℃; p_p=21325 Pa; v=0.29 m·s^{-1}; f=40 kHz). It could be seen that the feed side transfer coefficient of ultrasonic assisting VMD had the exponential growth relationship with the ultrasonic power. Consequently, the higher ultrasonic power was adopt preferentially when P<500W, the mass transfer effect on membrane surface (feed side) was perfectly. In addition, the implicit equation containing only K_f and P was also displayed in this figure. The correlation between experimental data and calculated value was fitted very well whatever for PP and PTFE hollow fiber membrane.

4.3.3 Effect of ultrasonic frequency to K_f

Fig. 11 showed that the feed side transfer coefficient of PP and PTFE hollow fiber membrane changed with ultrasonic frequency when operating under certain conditions (T_f=73℃; p_p=21325 Pa; v=0.29 m·s^{-1}; P=500W). It is obviously shown that the curves of ultrasonic frequency to feed side transfer coefficient was also divided into two parts. When the ultrasonic frequency was less than 40 kHz, the effect was positive; when the ultrasonic frequency was greater than 40 kHz, the effect was negative. This situation indicated that the transfer coefficient value was related to the strength of cavitation effect. The intensity of cavitation effect was determined by the size and amount of cavitation bubbles. In general, the amount of cavitation bubbles was positive correlation with the ultrasonic frequency increasing. However, the extravagant ultrasonic frequency will generate large amounts of small volume cavitation bubbles with lower collapse energy.

Fig. 12 showed the cubic polynomial fit for feed side transfer coefficient of PP and PTFE hollow fiber membrane changed with ultrasonic frequency when operating under certain conditions (T_f=73℃; p_p=21325 Pa; v=0.29 m·s^{-1}; P=500W). From this figure, the tendency of fit curve increased at first and then decreased when f>40 kHz. The results showed that the feed side transfer coefficient which is 13.09×10^{-7} kg·m^{-2}·s^{-1}·Pa^{-1} (PP) and 10.57×10^{-7} kg·m^{-2}·s^{-1}·Pa^{-1} (PTFE)
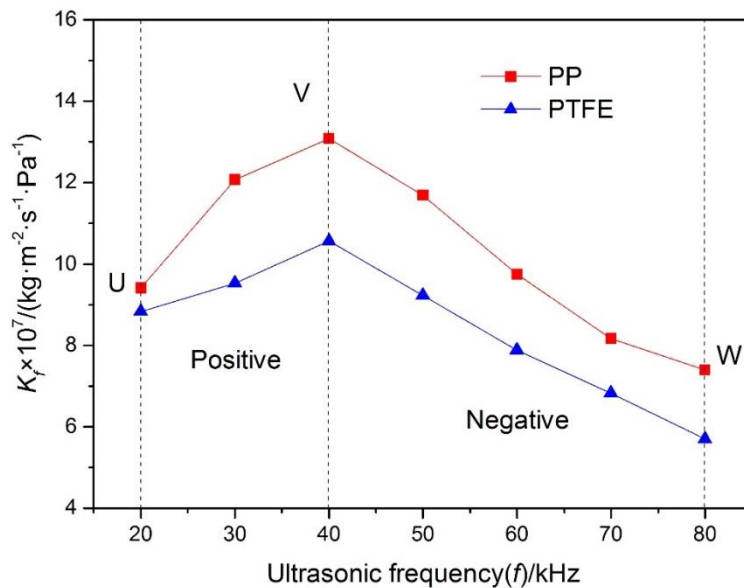

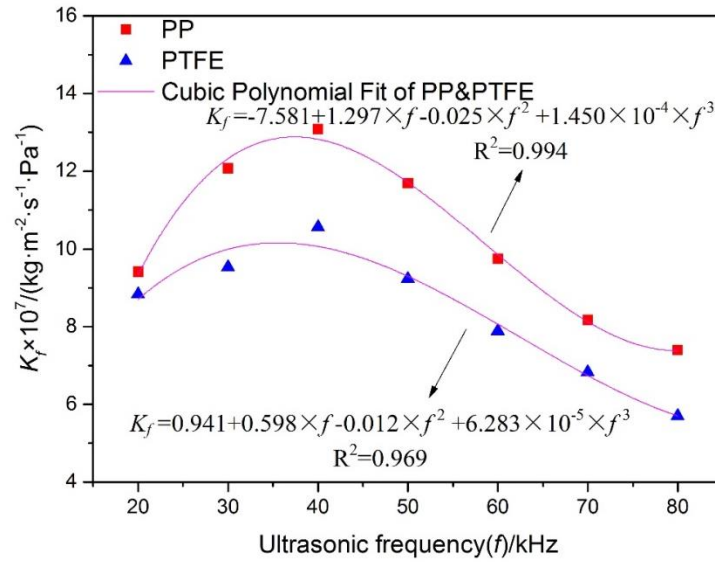Fig. 11 Effect of ultrasonic frequency to feed side transfer coefficient

Fig. 12 Relationship between feed side transfer coefficient and ultrasonic frequency
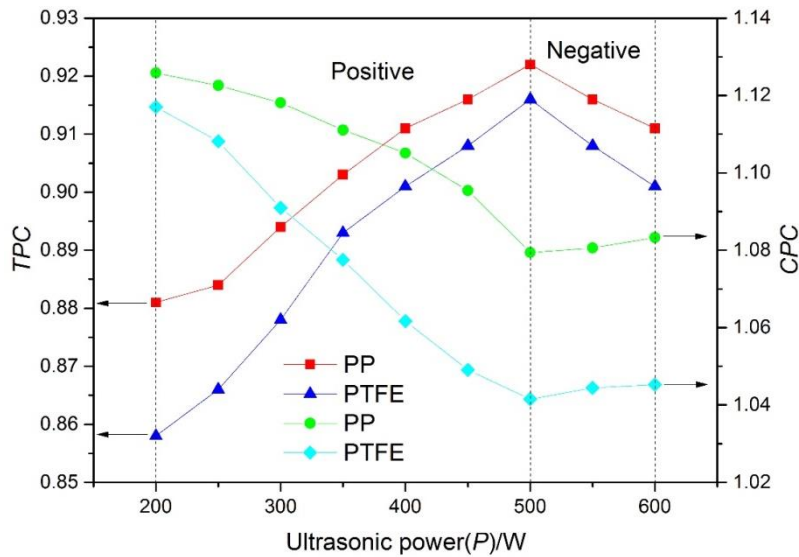

Fig. 13 Effect of ultrasonic power on *TPC* and *CPC*

reaches a maximum when the ultrasonic frequency is 40 kHz. In addition, the implicit equation containing only K_f and f was also displayed in this figure. The correlation between experimental data and calculated value was fitted very well whatever for PP and PTFE hollow fiber membrane.

4.4 Effect of ultrasonic parameters on TPC and CPC

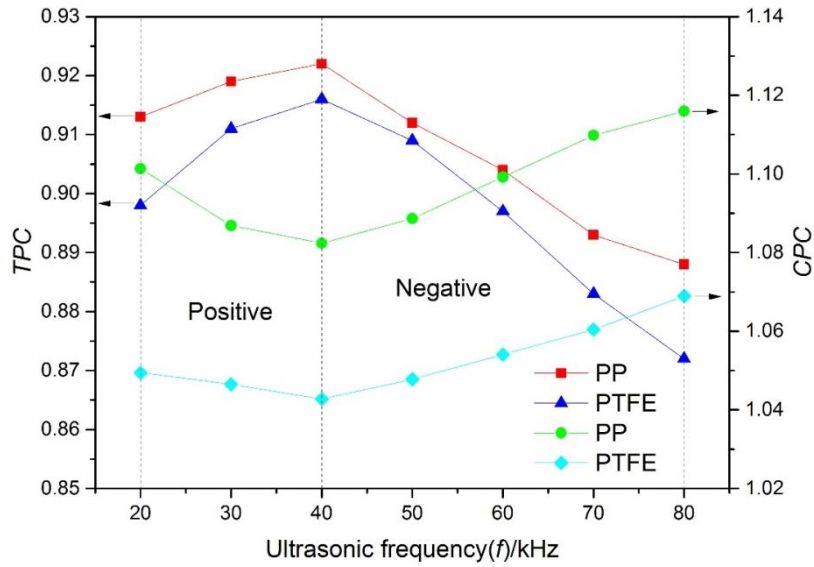### 4.4.1 Effect of ultrasonic power on TPC and CPC

Fig. 14 Effect of ultrasonic frequency on *TPC* and *CPC*

Fig. 13 showed TPC and CPC variation with the ultrasonic power when operating under certain conditions (T_f=73°C; p_p=21325 Pa; v=0.29 m·s^{-1}; f=40 kHz). In this figure, it could be seen that TPC increased and CPC decreased with increasing ultrasonic power (P<500W). When ultrasonic power is higher than 500W, its effect to TPC and CPC was opposite. This further demonstrated that heat transfer efficiency and mass transfer efficiency was unfavorable when adopting lower ultrasonic power. In addition, heat transfer effect and mass transfer effect was enhanced as the ultrasonic power increasing (P<500W). It was mainly because that the ultrasonic power could generate cavitation effect and higher shear stress acting on membrane surface (feed side) to reduce the thickness of concentration boundary layer.

4.4.2 Effect of ultrasonic frequency on TPC and CPC

Fig. 14 showed TPC and CPC variation with the ultrasonic frequency when operating under certain conditions (T_f=73°C; p_p=21325 Pa; v=0.29 m·s^{-1}; P=500W). In this figure, it could be seen that TPC and CPC value is much close to 1.0 when ultrasonic frequency is 40 kHz. In addition, TPC and CPC value was unsatisfactory when ultrasonic frequency greater than or less than 40 kHz. This further demonstrated that heat transfer efficiency and mass transfer efficiency was favorable when adopting applicable ultrasonic frequency. It was mainly because that the appropriate ultrasonic frequency could greatly intensify the heat and mass transfer process and diminish temperature polarization and concentration polarization effect in the boundary layer.

5. Conclusions

In this study, an ultrasonic assisting VMD system was designed to promote the heat and mass transfer in MD process. Both the effects of operating conditions and ultrasonic parameters to permeation flux in this process were investigated; the heat and mass transfer mechanism was also

been discussed. The conclusions of this paper have been summarized as follows.

• Ultrasonic assisting was an effective method to enhance the performance of VMD process. The permeation flux was improved at a certain operating conditions and ultrasonic parameters.

• No matter to PP and PTFE hollow fiber membrane, the permeation flux was boosted at a certain solution temperature, pressure at permeate side and feed solution velocity.

• According to the feed side transfer coefficient (K_f) correlation with the ultrasonic power and frequency in the experiment, the mathematical models were obtained as followed.

$$K_f = 4.406 - 0.026 \times P + 7.824 \times 10^{-5} \times P^2 \qquad\qquad R^2 = 0.998$$

$$K_f = 0.941 + 0.598 \times f - 0.012 \times f^2 + 6.283 \times 10^{-5} \times f^3 \qquad\qquad R^2 = 0.969$$

Based on the variation of TPC and CPC, the results showed that ultrasonic assisting was the key factor affecting TPC and CPC. Both of TPC and CPC were improved significantly with the optimal ultrasonic parameters.

Acknowledgments

References

Abu-Zeid, M.A.E.R., Zhang, L., Jin, W.Y., Feng, T., Wu, Y., Chen, H.L. and Hou, L.A. (2016), "Improving the performance of the air gap membrane distillation process by using a supplementary vacuum pump", *Desalinat.*, **384**, 31-42.

Al-Asheh, S., Banat, F., Qtaishat, M. and Al-Khateeb, M. (2006), "Concentration of sucrose solutions via vacuum membrane distillation", *Desalinat.*, **195**, 60-68.

Alkhudhiri, A., Darwish, N. and Hilal, N. (2012), "Membrane distillation: a comprehensive review", *Desalinat.*, **287**, 2-18.

Banat, F., Al-Asheh, S. and Qtaishat, M. (2005), "Treatment of waters colored with methylene blue dye by vacuum membrane distillation", *Desalinat.*, **174**, 87-96.

Banat, F., Al-Rub, F.A. and Bani-Melhem, K. (2003), "Desalination by vacuum membrane distillation: sensitivity analysis", *Sep. Purif. Technol.*, **33**, 75-87.

Cao, W.S., Liu, Q., Wang, Y.Q. and Mujtaba, I.M. (2016), "Modeling and simulation of VMD desalination process by ANN", *Comput. Chem. Eng.*, **84**, 96-103.

Chang, H.H., Tsai, C.H., Wei, H.C. and Cheng, L.P. (2014), "Effect of structure of PVDF membranes on the performance of membrane distillation", *Membr. Water Treat.*, **5**(1), 41-56.

Chen, Z.L., Rana, D., Matsuura, T., Meng, D. and Lan, C.Q. (2015), "Study on structure and vacuum membrane distillation performance of PVDF membranes: II. Influence of molecular weight", *Chem. Eng. J.*, **276**, 174-184.

Chen, Z.L., Rana, D., Matsuura, T., Yang, Y.F. and Lan, C.Q. (2014), "Study on the structure and vacuum membrane distillation performance of PVDF composite membranes: I. Influence of blending", *Sep. Purif. Technol.*, **133**, 303-312.

Cheng, P.G., Tang, N. and Wang, X.K. (2008), "Research on aqueous salt solution desalination by vacuum membrane distillation", *Chem. Ind. Eng. Prog.*, **27**(7), 1027-1031.

Chiam, C.K. and Sarbatly, R. (2013), "Vacuum membrane distillation processes for aqueous solution treatment - a review", *Chem. Eng. Proc.*, **74**, 27-54.

Crum, L.A. (1995), "Comments on the evolving field of sonochemistry by a cavitation physicist", *Ultrason. Sonochem.*, **2**(2), S147-S152.

Diban, N., Voinea, O.C., Urtiaga, A. and Ortiz, I. (2009), "Vacuum membrane distillation of the main pear aroma compound: experimental study and mass transfer modeling", *J. Membr. Sci.*, **326**, 64-75.

Efome, J.E., Baghbanzadeh, M., Rana, D., Matsuura, T. and Lan, C.Q. (2015), "Effects of superhydrophobic SiO$_2$ nanoparticles on the performance of PVDF flat sheet membranes for vacuum membrane distillation", *Desalinat.*, **373**, 47-57.

Efome, J.E., Rana, D., Matsuura, T. and Lan, C.Q. (2016), "Enhanced performance of PVDF nanocomposite membrane by nanofiber coating: A membrane for sustainable desalination through MD", *Water Res.*, **89**, 39-49.

El-Bourawi, M.S., Ding, Z., Ma, R. and Khayet, M. (2006), "A framework for better understanding membrane distillation separation process", *J. Membr. Sci.*, **285**, 4-29.

Fick, A. (1995), "On liquid diffusion", *J. Membr. Sci.*, **100**(1), 33-38.

Garcia-Payo, M.C., Essalhi, M., Khayet, M., Garcia-Fernandez, L., Charfi K. and Arafat, H. (2010), "Water desalination by membrane distillation using PVDF-HFP hollow fiber membranes", *Membr. Water Treat.*, **1**(3), 215-230.

Gryta, M. (2010), "Application of membrane distillation process for tap water purification", *Membr. Water Treat.*, **1**(1), 1-12.

Lawson, K.W. and Lloyd, D.R. (1996), "Membrane distillation (I): Module design and performance evaluation using vacuum membrane distillation", *J. Membr. Sci.*, **120**, 111-121.

Lawson, K.W. and Lloyd, D.R. (1997), "Membrane distillation", *J. Membr. Sci.*, **124**(1), 1-25.

Li, B.A. and Sirkar, K.K. (2005), "Novel membrane and device for vacuum membrane distillation based desalination process", *J. Membr. Sci.*, **257**, 60-75.

Liu, L.Y., Ding, Z.W., Chang, L.J., Tong, D.W. and Wei, R.Y. (2008), "Progress in membrane separation enhanced by ultrasound", *Chem. Ind. Eng. Prog.*, **27**(1), 32-37.

Loussif, N. and Orfi, J. (2014), "Effects of slip velocity on air gap membrane distillation process", *Membr. Water Treat.*, **5**(1), 57-71.

Loussif, N. and Orfi, J. (2016), "Comparative study of air gap, direct contact and sweeping gas membrane distillation configurations", *Membr. Water Treat.*, **7**(1), 71-86.

Mengual, J.I., Khayet, M. and Godino, M.P. (2004), "Heat and mass transfer in vacuum membrane distillation", *Int. J. Heat Mass Tran.*, **47**, 865-875.

Mericq, J.P., Laborie, S. and Cabassud, C. (2011), "Evaluation of systems coupling vacuum membrane distillation and solar energy for seawater desalination", *Chem. Eng. J.*, **166**, 596-606.

Porter, M.C. (1972), "Concentration polarization with membrane ultrafiltration", *Ind. Eng. Chem. Prod. Res. Develop.*, **11**(3), 234-248.

Schofield, R.W., Fane, A.G. and Fell, C.J.D. (1987), "Heat and mass transfer in membrane distillation", *J. Membr. Sci.*, **33**(3), 299-313.

Thompson, L.H. and Doraiswamy, L.K. (1999), "Sonochemistry: science and engineering", *Ind. Eng. Chem. Res.*, **38**, 1215-1249.

Wang, P., Zhao, J., Chen, H.Y. and Lv, X.L. (2014), "Heat and mass transfer in osmotic distillation", *Chem. Ind. Eng. Prog.*, **65**(8), 2889-2895.

Xu, Y., Zhu, B.K. and Xu, Y.Y. (2006), "Pilot test of vacuum membrane distillation for seawater desalination on a ship", *Desalinat.*, **189**, 165-169.

Yang, Y.F., Rana, D., Matsuura, T. and Lan, C.Q. (2016), "The heat and mass transfer of vacuum membrane distillation: Effect of active layer morphology with and without support material", *Sep. Purif. Technol.*, **164**, 56-62.

Yang, Y.F., Rana, D., Matsuura, T., Zheng S.Y. and Lan, C.Q. (2014), "Criteria for the selection of a support material to fabricate coated membranes for a life support device", *RSC Adv.*, **4**(73), 38711-38717.

RJ

Nomenclatures

u	superficial velocity ($m \cdot s^{-1}$)
M	molecular weight of water ($kg \cdot kmol^{-1}$)
d	inner diameter of hollow fiber membrane (m)
D	external diameter of hollow fiber membrane (m)
r	membrane pore radius (m)
T	average temperature (K)
J	permeation flux of VMD ($kg \cdot m^{-2} \cdot h^{-1}$)
Q	thermal energy (W)
K	mass transfer coefficient ($kg \cdot m^{-2} \cdot s^{-1} \cdot Pa^{-1}$)
p	water vapor pressure (Pa)
h	heat transfer coefficient ($W \cdot m^{-2} \cdot K^{-1}$)
R	universal gas constant ($J \cdot kmol^{-1} \cdot K^{-1}$)
A	area (m^2)
l	effective length of the membrane module (m)
ΔH	latent heat of water evaporation ($J \cdot kg^{-1}$)
C_p	heat capacity at constant pressure ($J \cdot kg^{-1} \cdot K^{-1}$)
P	ultrasonic power (W)
f	ultrasonic frequency (Hz)

Greek symbols

μ	dynamic viscosity ($kg \cdot m^{-1} \cdot s^{-1}$)
ρ	density of the fluid ($kg \cdot m^{-3}$)
ε	porosity of the membrane (-)
δ	membrane thickness (m)
τ	pore tortuosity (-)
λ	thermal conductivity ($W \cdot m^{-1} \cdot K^{-1}$)

Subscripts

m	membrane inside
f	feed side
p	permeate side
fm	membrane surface on the feed side
pm	membrane surface in the permeate side